Ceramics-Silikáty 62 (2), 146-157 (2018)
www.ceramics-silikaty.cz doi: 10.13168/cs.2018.0006

CORROSION AND OXIDATION BEHAVIOR OF POLYMER DERIVED CERAMIC COATINGS WITH PASSIVE GLASS FILLERS ON AISI 441 STAINLESS STEEL

#M. PARCHOVIANSKÝ*, I. PETRÍKOVÁ*, G.S. BARROSO**, P. ŠVANČÁREK*, D. GALUSKOVA*, G. MOTZ**, D. GALUSEK*

*Vitrum Laugaricio – Joint Glass Center of the IIC SAS, TnU AD, and FCHFT STU, Študentská 2, 911 50 Trenčín, Slovakia
**University of Bayreuth, Ceramic Materials Engineering, D-95440 Bayreuth, Germany

#E-mail: milan.parchoviansky@tnuni.sk

Submitted September 4, 2017; accepted January 31, 2018

Keywords: PDC ceramics, Glass microspheres, Hydrothermal corrosion, High temperature oxidation

Polymer derived ceramic (PDC) polysilazane-based double layer composite coatings on steel substrates consisting of a PDC bond-coat, and a PDC-based top-coat containing ceramic passive (ZrO_2) and active ($ZrSi_2$) fillers, as well as a specially tailored passive glass filler with high melting temperature were developed. The corrosion and oxidation behaviour of the ferritic stainless steel AISI 441 with and without the PDC coating system was evaluated. SEM examination revealed the composite coatings were not dense but contained small closed pores with a diameter up to 100 nm. Cracks and occasionally also delamination were detected. The static corrosion tests under hydrothermal conditions at the temperature of 200°C resulted in partial oxidation of the uncoated steel substrate, whereas the coated sample was protected by the PDC coating. No oxidation of the top coat was detected after the static corrosion test. The high temperature oxidation behaviour in a flow-through oxygen atmosphere was investigated at the temperatures of 900°C, 1000°C and 1100°C. X-ray diffraction confirmed extensive corrosion of the uncoated AISI 441 stainless steel accompanied by formation of a Cr_2O_3, TiO_2 and a $(Mn, Cr)_3O_4$ spinel containing layer of corrosion products. Beneficial effect of the PDC coating was observed at the temperature of 900°C, demonstrated by marked reduction of the weight gain of coated steel after 196 h of exposure to flowing oxygen. At higher temperatures the protective action of the PDC coat was not observed, and a thick layer of corrosion products was formed at the steel/coating interface.

INTRODUCTION

From economic point of view the ferritic stainless steel AISI 441 is a suitable material for a variety of applications. However, the corrosion and oxidation performance of the steel is not sufficient for a long-term operation at higher temperatures [1]. A non-protective $(Mn,Cr)_3O_4$ spinel layer is formed at the surface when the steel is exposed to oxidation environment at T > 800°C, together with a protective Cr_2O_3 underneath the $(Mn,Cr)_3O_4$ spinel layer [2]. Some authors report that the oxide film is composed of chromia (Cr_2O_3) or chromium-rich iron oxide ($(Cr,Fe)_2O_3$) in the inner part and by a manganese-chromium spinel oxide $(Mn,Cr)_3O_4$ in the outer part [3, 4]. At the metal/oxide interface, a silica (SiO_2) layer is also typically observed [5]. In order to increase life-time of steel parts and components their surfaces have to be protected in order to prevent formation of the oxide layer and to avoid oxide scale growth.

The high temperature corrosion and oxidation resistance of stainless steel can be enhanced by polymer derived ceramic coatings [6], which offer a number of advantages in comparison to traditional methods of ceramic processing, especially easy application on substrates of any shape by simple lacquer methods like dip-coating [7], spray-coating [8, 9] or spin-coating [10] as well as by typical ceramic shaping methods like tape-casting [11]. They are also specific by low temperature processing and the potential to tailor the properties via microstructure and composition design. Polymer derived ceramic (PDC) composite coatings are promising candidates to be used as alternative environmental barrier coatings for corrosion and oxidation protection of metals [12]. A new approach based on development of oxidation resistant PDC coating systems through pyrolysis of suitable predominantly silicon containing precursors such as polysiloxanes [13], polycarbosilanes [14] or polysilazanes [15, 16, 17], which could act as a diffusion barrier to oxygen was reported. The precursor techniques facilitate relatively low-cost and easy approach to produce polymeric and ceramic coatings, which in turn provide excellent oxidation and corrosion protection of metal substrates.

The greatest disadvantage of PDCs processing is the shrinkage of polymer during pyrolysis, which can be higher than 50 % by volume [18]. The performance of PDC coatings is also affected by thermal expansion mismatch between the ceramic and the metal, thermal stresses generated by temperature gradients, as well as residual stresses arising from the deposition process [19]. Residual stresses caused by the high volume shrin-

kage lead to the formation of defects, cracks or even delamination of the coatings. Although PDC can provide a significant level of oxidation protection for steel, the protective effect is markedly reduced if the coatings are too porous or contain cracks. A double layer coating consisting of a polymer derived ceramic (PDC) bond coat, and a PDC top coat with glass and ceramic fillers appears to be an efficient solution of the problem [20]. The bond coat can increase adhesion for mechanical bonding of the ceramic top coat, protects the underlying steel substrate against the high temperature oxidation and corrosion, and reduces the CTE mismatch between the steel substrate and ceramic top coat materials. Key issue to produce defect free coatings is the reduction of shrinkage and porosity formation by adding passive or active fillers [21], which partially or completely eliminates the volume change due to polymer to ceramic conversion. A number of authors figured out that the incorporation of passive fillers like BN [22], ZrO_2 [23] or Al_2O_3 [24] can decrease the volume fraction of shrinking while reactive filler particles like $ZrSi_2$ [25] or $TiSi_2$ [26, 27] can compensate the shrinkage of pre-ceramic polymers through reactions with the polymer decomposition products and formation of products with higher specific volume. Furthermore, depending on the properties of the substrate, the thermal expansion coefficient of the coatings can be adjusted by an adequate filler material. Moreover, by incorporation of glass fillers it is also possible to generate coatings with additional functionalities and increase the efficiency as environmental barrier coating [28].

This work was therefore aimed at development of a modified corrosion and oxidation resistant coating system with protective action at elevated temperatures around 1000°C. For that purpose, a double layer coating, consisting of a PDC bond-coat, and a PDC top-coat with ceramic and specially tailored glass fillers (SiO_2–Al_2O_3–ZrO_2) in the form of microspheres with high melting temperature were prepared and studied from the point of view of their corrosion and oxidation resistance. Uncoated substrate (ferritic steel grade AISI 441) was used as a reference. The rate of oxidation in pure flow-through oxygen atmosphere was determined, and the oxide scales formed after different exposures times and temperatures on coated and uncoated samples were characterized by SEM/EDS and XRD, including detailed microstructural and phase analysis of the oxide scales formed in the atmosphere of oxygen.

EXPERIMENTAL

Two different commercially available polysilazanes, PHPS (perhydropolysilazane) and Durazane 1800 (both Merck KGaA, Germany), were used as preceramic precursors for the coating procedure. PHPS is produced by ammonolysis of dichlorosilane (SiH_2Cl_2), while the precursor Durazane 1800 is a liquid (organo) silazane synthesized by co-ammonolysis of dichloromethylvinylsilane (H_2C=$CHSi(CH_3)Cl_2$) and dichloromethylsilane (CH_3SiHCl_2). Stainless steel (AISI 441) was cut into sheets with the dimensions of 10 × 10 mm, ultrasonically cleaned in acetone and dried. The bond-coat was prepared from PHPS by dip-coating of the cleaned metal sheets (dip-coater RDC 15, Relamatic, Switzerland) with a hoisting speed of 0.3 $m \cdot min^{-1}$. The pyrolysis of the bond-coat was performed in air at a temperature of 500°C for 1 h with heating and cooling rates of 5 $K \cdot min^{-1}$ (Nabertherm® *N41/H,* Nabertherm, Germany). For the top-coat, yttria-stabilized zirconia (YSZ) (H. C. Starck GmbH, Germany) with D90 = 0.50 μm, D50 = 0.3 μm was used as passive filler, while zirconium disilicide ($ZrSi_2$, ball-milled to D90 = 3 μm, D50 = 1.5 μm, HMW, Germany) was used as active filler. A combination of reactive and inert fillers was used to stabilize a homogeneous distribution of the additives both in the solution and in the resulting coating. The top-coat was prepared by mixing the ceramic filler particles YSZ (64.8 vol. %), $ZrSi_2$ (5.4 vol. %), and glass microspheres (3.4 vol. %) with the composition (in mol. %) $80SiO_2$–$10Al_2O_3$–$10ZrO_2$, prepared by flame synthesis, with the liquid (organo)silazane Durazane 1800 (26.3 vol. %). To improve the cross-linking behaviour of the Durazane 1800 at low temperatures, 3 wt. % of DCP (dicumyl peroxide, Sigma–Aldrich Chemie GmbH, Germany) was added to the polymer. The YSZ, $ZrSi_2$ and the glass fillers were separately dispersed in a solution of di-*n*-butylether with added dispersant (DISPERBYK 2070, BYK-Chemie GmbH, Germany), followed by 30 min ultrasonic treatment and stirring overnight. Then the liquid polysilazane Durazane 1800 was added and the resulting mixture was applied by spray-coating technique. The pyrolysis of the composite coatings was performed in air (Nabertherm® *N41/H,* Nabertherm, Germany) at 1000°C with the heating and cooling rate of 3 $K \cdot min^{-1}$ and a holding time of 1 h.

The hydrothermal corrosion tests were performed in Teflon-lined pressure corrosion reactors with the inside volume of 26 cm^3 filled with deionized water as a corrosion liquid and heated in laboratory drying oven. Static tests were carried out at the temperature of 200°C with the duration of the test between 1 and 8 days. The ratio between the sample surface and the volume of corrosive liquid (S/V) was held constant at 0.7 ± 0.03 cm^3. For determination of each experimental data point two specimens were placed in one reactor with 20 ml of the corrosion medium. The corrosion medium was not changed during the whole duration of the test.

High temperature oxidation tests were carried out in a high temperature horizontal electric tube furnace (Clasic 0213T, Clasic, Praha, Czech Republic) at the temperatures of 900°C, 1000°C and 1100°C and the exposure times in the range of 1 - 96 hours in flowing oxygen (purity 99.5 %, Linde, Slovakia). The furnace was heated to the preset temperature at a heating rate

of 10 $K \cdot min^{-1}$, and the samples isothermally heated under the specified conditions for a pre-defined period of time. After each test the coated and uncoated samples were weighted and specific weight changes related to the samples' surface area were calculated in order to investigate the role of the coating during oxidation.

Microstructure of both hydrothermally corroded and oxidized samples (coated and uncoated) was in detail examined by scanning electron microscopy (JEOL JSM 7600 F, JEOL, Japan) equipped with EDS detector (Oxford Instruments, UK). X-ray powder diffraction analysis (CuK_α, 2θ range 10 - 80°, Empyrean DY1098, PANalytical B.V., Netherlands) was used to detect any secondary phases, which could result from chemical reactions between the components of the steel substrate, coating and corrosive agents. The monoclinic volume fractions (V_m) of YSZ after corrosion tests were calculated according to the equation proposed by Garvie and Nicholson [29] and modified by Toraya [30]:

$$Vm = \frac{1.311 \times Xm}{1 + 0.311 \times Xm}, \text{ with } Xm = \frac{I_m^{111} + I_m^{\bar{1}11}}{I_m^{111} + I_m^{\bar{1}11} + I_t^{101}} \quad (1)$$

where I_p^{hkl} are the areas (integral intensities) of diffraction peaks related to the respective (hkl) planes of phase p (m for monoclinic and t for tetragonal). With the measurement conditions used, the sensitivity of this method is approximately 1 % for both materials.

RESULTS AND DISCUSSION

Characterisation of the coatings

After pyrolysis in air at 1000°C the glass filled polysilazane-based coatings contain, as detected by XRD, two crystalline phases, namely monoclinic and tetragonal ZrO_2. The zirconia possibly created by crystallization of glass fillers could not be distinguished from ZrO_2 added deliberately as the passive filler or ZrO_2 formed as a product of oxidation of zirconium disilicide in the course of pyrolysis. The results also indicate that no chemical interactions between the HTT1800 polysilazane and the zirconia/glass fillers resulting in the formation of new phases took place during the pyrolysis. Both glass microspheres and zirconia can be thus considered as passive fillers. Figure 1a, b shows the SEM micrographs of top coatings on stainless steel: the SEM examination was focused on evaluation of homogeneity, adhesion and possible failures of the coatings before corrosion and oxidation tests. Furthermore, the cross-sectional micrograph (Figure 1b) with the EDX analysis of coated samples at the metal–ceramic interface was obtained to investigate the bonding between the substrate and the coating. The composite coatings were uniform and well adherent. ZrO_2 particles were distributed homogeneously in the matrix. In some cases glass microspheres were also observed (Figure 1a) with the diameter of approximately 10 μm. However, the composite coatings were not fully dense, contained small closed pores with a diameter up to 100 nm. In some cases, cracks and occasionally also delamination (Figure 1a) were detected both within and at the interface of the approximately 10 μm thick coatings, due to high volume shrinkage of the precursor during pyrolysis. This problem is already known from the processing of enamels, where the formation of pores in general cannot be completely avoided. The pores result from the release of gases, which are generated from the conversion of the polysilazane HTT 1800 and from the decomposition of the dispersant and/or other organic species in processing additives. Since the diameter of the pores lies in the range of the coating thickness, such coatings do not possess environmental barrier properties. On the other hand, the high magnification SEM cross-section (Figure 1b) view shows strong bond at the interfaces between metal/PHPS and PHPS/top coat. Due to the reactivity of the PHPS, direct chemical bonds between the stainless steel substrates and the PHPS were formed. The PHPS-based bond coat increased the adhesion of top coatings

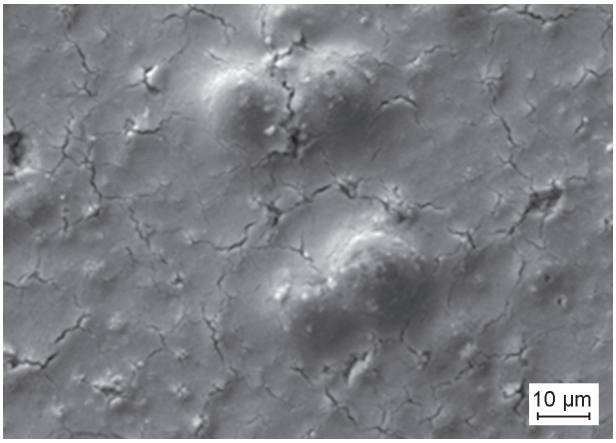

a)

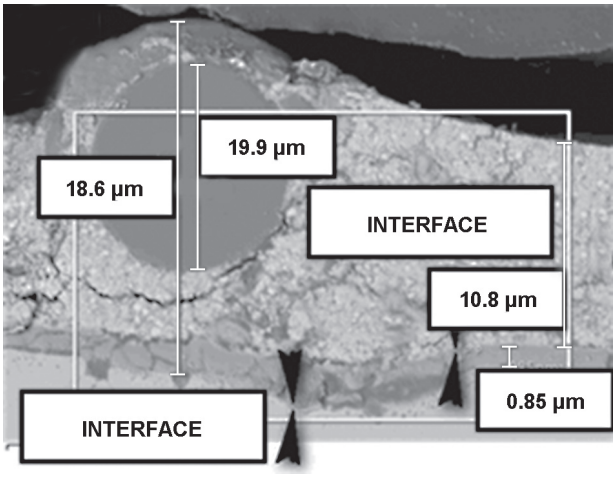

b)

Figure 1. SEM micrographs of the C-80-10-10 coating before corrosion and oxidation tests: a) surface, b) high resolution cross-section with embedded glass microsphere.

and acted as a diffusion barrier against oxidation during the pyrolysis of the coating system. Moreover, from the cross-section (Figure 1b) it can be seen that the cracks are lateral, propagating inside the ceramic layer along the ceramic/metal interface. Such orientation of cracks indicated at least some protection of the steel substrate.

Hydrothermal corrosion

In order to investigate the environmental protection ability of the coatings, static corrosion tests in deionized water were conducted at 200°C. Figures 2a-c shows the SEM micrographs of steel and the top coat after the corrosion test. Although the coatings were not fully dense, the static corrosion oxidation tests delivered some promising results. As shown in Figure 2a, the uncoated steel substrate was partially oxidized after corrosion at 200°C, whereas the coated sample (Figure 2b) was protected by the PDC coating. Application of the static conditions caused irregular growth of the oxide layer visible at the metal surface (Figure 2a), identified as the mixture of iron and chromium oxide: the EDS analysis detected Fe (37.7 at. %), Cr (9.7 at. %) and O (52.3 at. %). No visible degradation of the top coat substrate was detected after the static corrosion test. However, the fraction of monoclinic ZrO_2 increased from 67 vol. % to more than 70 vol. %, which indicates partial destabilization and transformation of Y-PSZ filler as a result of 96 h exposure to deionized water at 200°C. Moreover, randomly distributed spherical craters approximately 10 μm in diameter can be seen at the surface of the top coat, formed due to pull-out of glass microspheres (Figure 2b). This can be attributed to the difference of thermal expansion coefficients of the glass filler and the PDC matrix. Due to high silica content the estimated thermal expansion coefficient of the glass microspheres (2.3×10^{-6} K^{-1}) was lower than the thermal expansion coefficient of the composite coating. Residual compressive stresses were then created at the microsphere/coating interfaces: this and the absence of chemical bonding between coating and the glass filler resulted in preferential dissolution of material at the glass/coating boundary and eventual pull-out of microspheres from the ceramic layer.

However, the cross-section of the composite coating system with a thickness of about 15 μm (Figure 2c) shows that the coatings were not well adherent and contained cracks, which occasionally penetrated as deep as to the metal surface. The corrosive medium (water) could thus penetrate through the defects (i.e. pores and cracks in the coating) to the metal/coating interface, which was then attacked by corrosion and the coating didn't act as an efficient anti-corrosion barrier. For such type of coating, at least some oxidation/corrosion is expected to take place under the protective layer, directly at the steel surface due to restricted access of the corrosive medium to the steel surface. However, the absence of corrosion products at the surface of the PDC is only the proof of durability of the layer itself, not of its protective function, and the protective function of the coating has to be evaluated exclusively on the basis of the presence of metal (Cr, Fe, Mn) oxide layer at the metal-coating interface.

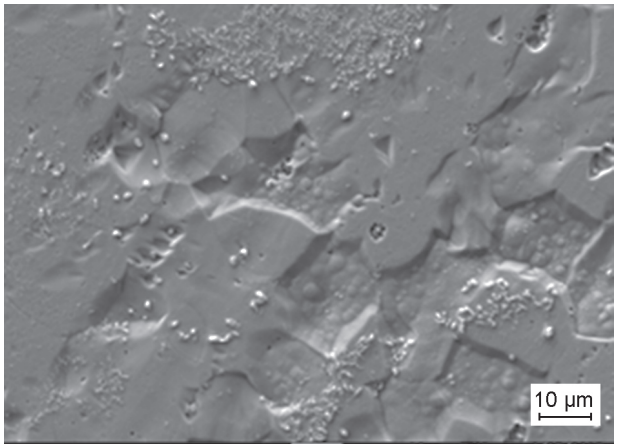

a) steel after 8 days

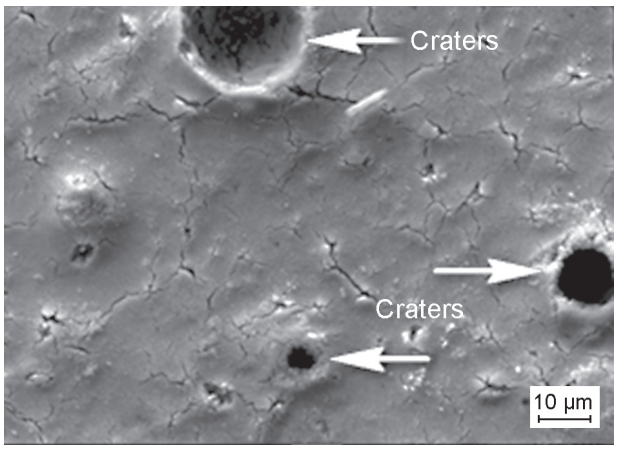

b) C-80-10-10 after 8 days

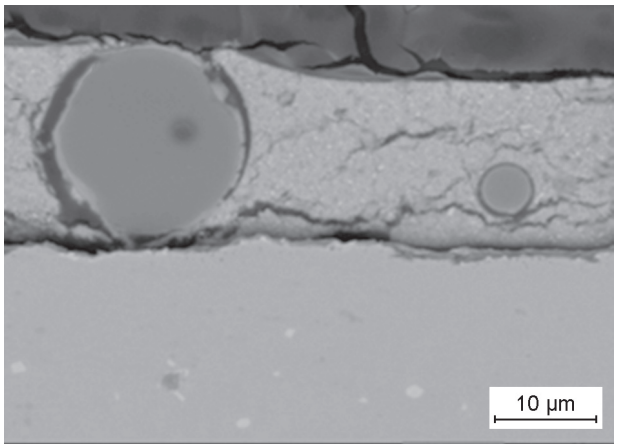

c) cross-section of C-80-10-10 after 8 days

Figure 2. SEM micrographs of steel and top coat after corrosion: a) steel after 8 days, b) C-80-10-10 after 8 days, c) cross-section of C-80-10-10 after 8 days.

High temperature oxidation

The oxidation tests were carried out at the temperatures 900°C, 1000°C and 1100°C with the isothermal dwell time ranging from 1 to 96 hours. After each test the coated and uncoated samples were weighted and weight changes were calculated in order to evaluate protective action of the coating during oxidation tests. Figure 3 and Figure 4 show the weight gain of the uncoated and coated steel, respectively, as a function of time at various temperatures. The oxidation rate is enhanced when the test temperature is increased from 900 to 1100°C, with a larger increase when the temperature was increased from 1000 to 1100°C. It is observed that the mass gain at all temperatures increases very rapidly at the initial stage probably due to rapid nucleation of oxide. The initial time dependence of weight gain of uncoated steel (Figure 3) due to the surface oxide scale growth approximately followed the classic Wagner parabolic relationship [31]. It is widely accepted the oxidation kinetics of stainless steel can be described by parabolic diffusion law:

$$\Delta m^2 = k_p t \qquad (2)$$

where Δm is the weight gain, t is the oxidation time and k_p is the parabolic rate constant.

Furthermore, the mass gain curves changed with the temperature, showing strong temperature dependence of the steel oxidation rates, but also a strong deviation from parabolic law at the latter stages of the oxidation test. According to the shape of curves, the oxidation processes of stainless steel under different testing conditions can be divided into different stages. Partial compliance with the parabolic law indicates that the high temperature oxidation kinetics of metals at the initial stage is controlled by the diffusion of cationic or anionic species through the oxide scale. At 900°C, the curve of the AISI 441 steel presents a tendency of linear law, following a steady state after 48h of oxidation. At 1000°C and 1100°C, the oxidation rates have an abrupt increase within 1h, following a parabolic regime, after which the oxidation reached the steady state observed for all 48 to 96 h cases. It is known that the kinetics of oxidation and the main reaction products change with temperature and time. The initial and incubation period can be explained as follows. The weight gain initially showed a sharp increase, up to 1 h of oxidation and subsequently showed negligible weight gain after the exposure period of 24 h. It means that the oxide growth is characterized by a rapid increase at the beginning, and then slowed down as the weight gain appearing to level off after 12 h, which indicates the trend for parabolic kinetics. The transport of the reactants of the oxidation process determines the rate of oxidation. In the initial period (up to 1 h), a faster rate of oxidation kinetics prevails until the nucleation and growth (and subsequent morphology) of oxides become organized. The minimal weight gain after exposure to 24 h signifies that the high temperature oxidation rate decreases with time and thus, the overall oxidation kinetics is likely to follow the parabolic growth law. In this case, the initially developed oxide scale controls and/or acts as a diffusion barrier to the ionic (metal cations and oxygen anion) transport during the later stage of oxidation process which causes the decreased rate of oxidation at longer exposure times, i.e. by continuing the oxidation, diffusion becomes the rate controlling process and the growth rate becomes parabolic. The oxidation kinetics after long exposure times (48 h) cannot be described in terms of parabolic law, neither for steel, nor coated samples. In the case of the coated steel parabolic kinetic in the initial stages of oxidation could be also observed. Similarly to uncoated samples, marked deviation from parabolic kinetics was observed at longer oxidation times, at higher temperatures with significantly lower mass gains than predicted from parabolic law kinetics. At 900°C the mass gain was about one half of the uncoated steel (Figure 4). The general trend of decreasing oxidation rate with increasing exposure time may be an indication of decreasing effective surface

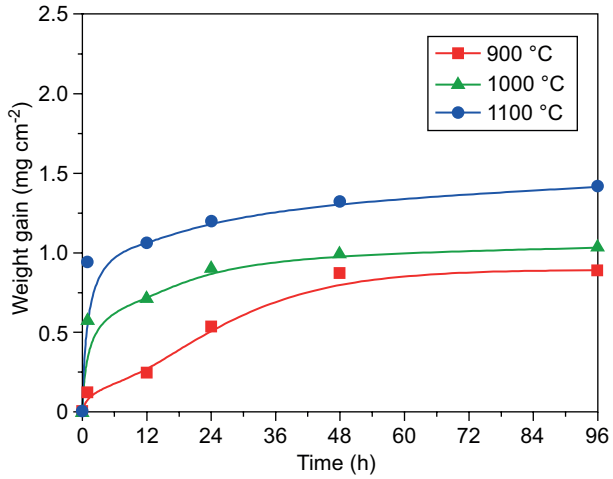

Figure 3. Mass gain of an AISI 441 steel substrate at various temperatures and different holding times.

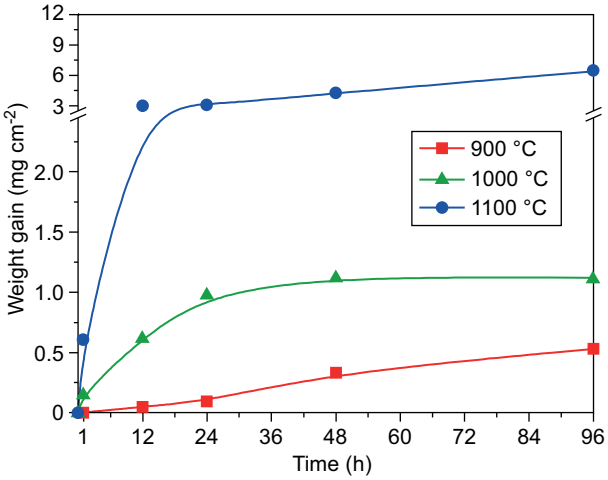

Figure 4. Mass gain of the coated steel substrate at various temperatures and different holding times.

areas of the bond coatings due to closure of small micropores and voids by the growing scale. It seems that the coating provides some protection at this temperature. However, at higher temperatures the mass gain of uncoated steel was lower than the weight gain measured for coated samples. Higher mass gain of coated steel can be explained as follows. Since the coatings were porous, they could not act as an efficient diffusion barrier to oxygen: the observed weight change of the coated samples was attributed to oxygen ion inward diffusion through the coating accompanied by its oxidation. The oxygen reacted with Si–N bonding of the pyrolysed polysilazane, additionally yielding more silica. The $ZrSi_2$ represented another source of mass increase, which resulted from complete conversion of $ZrSi_2$ to ZrO_2 and SiO_2. After this concurrent first oxidation steps, further mass increase in the coating occurred, mainly due to the oxidation of free Si to SiO_2. At higher temperatures (> 1000°C) $ZrSiO_4$ started to be formed and the product of the complete oxidation of $ZrSi_2$ was a mixture of $ZrSiO_4$, amorphous and crystalline SiO_2 and residual ZrO_2 [32]. After all available reaction sites were consumed by the oxidation reactions (incubation period at the mass gain-time dependence of coated steel at 900°C in the time interval 1 - 24 h, Figure 3) the oxygen diffused directly to the steel substrate, resulting in further oxidation of metallic elements from the steel. At higher temperatures all reaction sites in the coating were consumed quickly, resulting in almost immediate oxidation of metallic substrate.

The surface of oxidized specimens was analyzed by XRD to identify new phases formed during oxidation. SEM/EDS studies were carried out on the surface and scale cross sections to reveal any changes in the microstructure and the chemistry of steel and the coating, and the underlying substrate oxidized in oxygen at elevated temperatures and different holding times. In XRD patterns (Figures 5a-f) of stainless steel substrate Fe, Cr_2O_3, TiO_2 and spinel $(Mn,Cr)_3O_4$ were identified. The Rietveld analysis was used to quantitatively determine the amount of oxide phases at corroded steel and coating surfaces (Figures 5a-f). Presence of the $(Mn,Cr)_3O_4$ spinel at the surface of uncoated steel substrate refers to ferritic stainless steel that normally contains small amounts of Mn. When ferritic stainless steel is subjected to the higher temperature > 800°C, the spinel $(Mn,Cr)_3O_4$ layer can be formed. Also a protective Cr_2O_3 layer is formed underneath the $(Mn,Cr)_3O_4$ spinel layer. This fact also indicates that the oxidation kinetics of steel grade AISI 441 under the applied conditions was in initial time periods controlled by an outward diffusion of Cr^{3+} cations in the Cr_2O_3 scale.

The formation of a $(Mn,Cr)_3O_4$ spinel in contact with a manganese-containing Cr_2O_3 scale is in agreement with the known phase relationships at this temperature, as determined by Badin et. al. [3] The precipitation of the $(Mn,Cr)_3O_4$ spinel on the top of the Cr_2O_3 scale can be attributed to high diffusion coefficient of manganese ions and strong affinity with oxygen. The metal ion diffusion decreases in the order of $D_{Mn} > D_{Fe} > D_{Cr}$ by assuming that these metals ions diffuse via Cr^{3+} lattice sites in Cr_2O_3 [33]. Mn-spinels, forming most of the external layer, can reduce Cr activity and stabilize the oxidation rate. Moreover, these spinels forming at the gass-scale interface are very likely to diminish the oxygen pressure applied on the main layer and thus to help to reach the steady state of oxidation observed for all 48 to 96 h cases. Not only the diffusion of chromium and oxygen in the Cr_2O_3 layer are of interest but also the diffusion of cations and transport of non-metal elements. The outward diffusion of cations such as $Fe^{2+/3+}$, Mn^{2+} from the steel through the chromia layer plays a role in the growth of the outer spinel layer in the oxidation process of steel. Mn is mainly oxidized as Mn^{2+} such as in MnM_2O_4 with

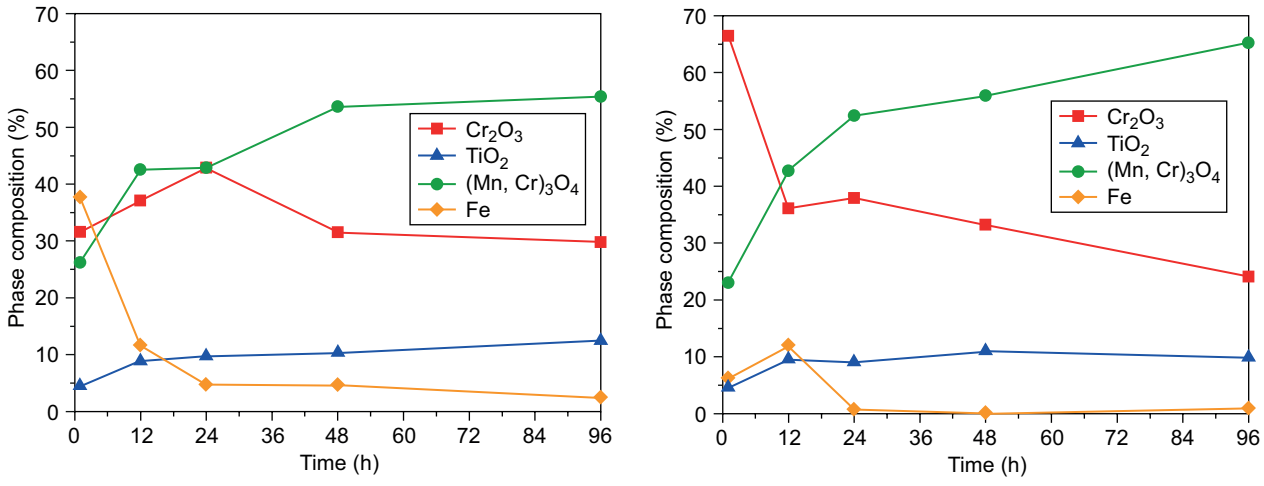

a) steel – 900°C b) steel – 1000°C

Figure 5. Time dependence of phase composition of oxidized sample obtained by Rietveld refinement of X-ray diffraction data of uncoated steel and C 80-10-10 coated steel substrate; a) steel – 900°C, b) steel − 1000°C. *(Continue on next page)*

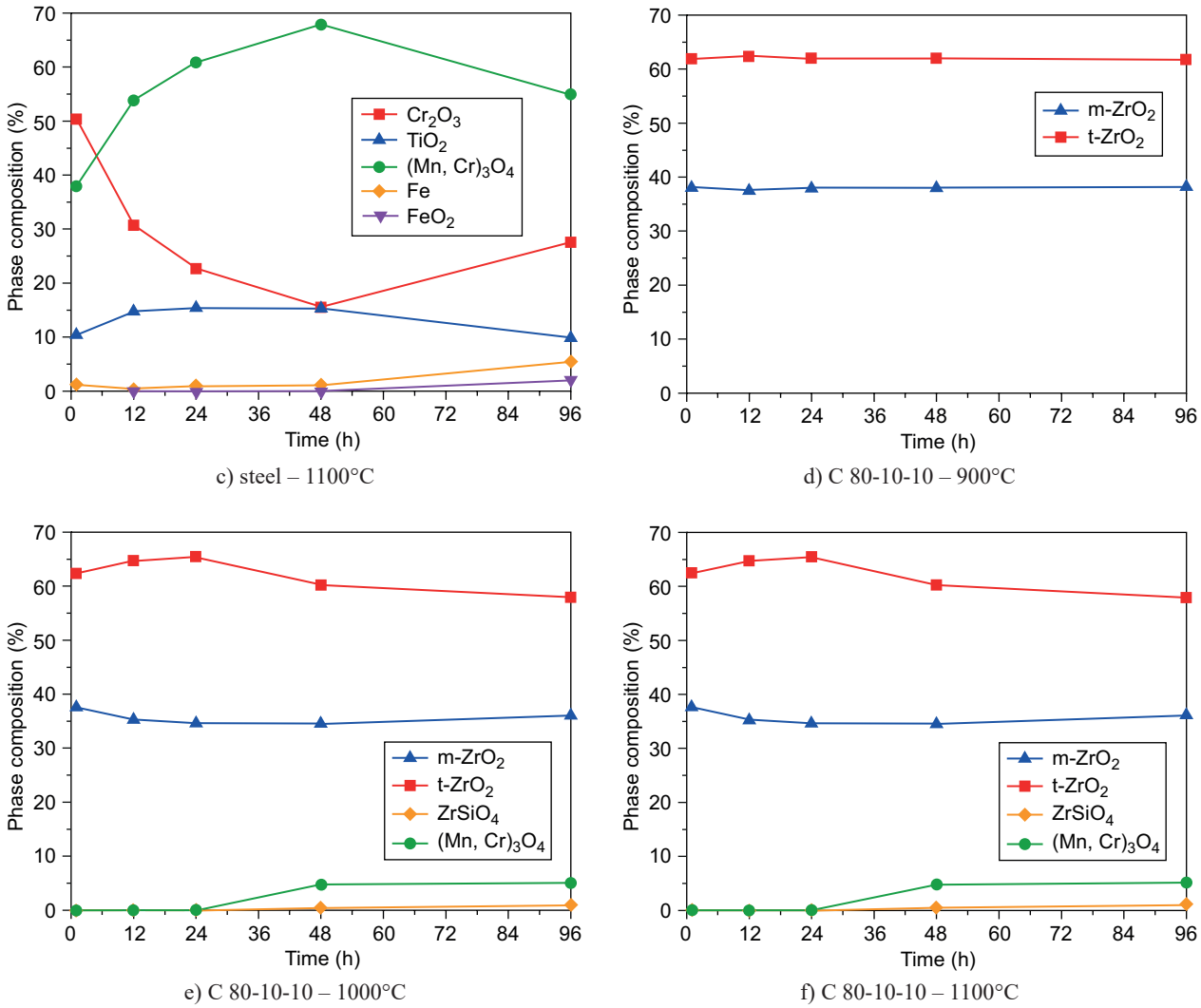

c) steel – 1100°C

d) C 80-10-10 – 900°C

e) C 80-10-10 – 1000°C

f) C 80-10-10 – 1100°C

Figure 5. Time dependence of phase composition of oxidized sample obtained by Rietveld refinement of X-ray diffraction data of uncoated steel and C 80-10-10 coated steel substrate; c) steel – 1100°C, d) C 80-10-10 – 900°C, e) C 80-10-10 – 1000°C, f) C 80-10-10 – 1100°C.

M being Cr or Fe. Fe shows signs of both Fe^{2+} and Fe^{3+}. From Auger Electron Spectroscopy measurements on growing Cr_2O_3 scale, Wild [34] concluded that Mn^{2+} ions diffuse two orders of magnitude faster than Cr^{3+} ions. Lobnig et al. [35] confirmed the very fast diffusion of Mn^{2+} ions in Cr_2O_3 scales by a direct diffusion experiment. Because of the fast diffusion of Mn^{2+} ions in oxide scales from steel to the scale surface, spinel is formed on oxide scales mainly composed of Cr_2O_3.

In the case of coated samples at the temperature of 900°C, the dominant phases are monoclinic and tetragonal ZrO_2 indicating nearly complete conversion of the active $ZrSi_2$ filler in the coating. In addition, as described earlier, the total oxidation of $ZrSi_2$ takes place at higher temperatures (> 1000°C) and is followed by the formation of $ZrSiO_4$, as confirmed by XRD (Figures 5e-f). At the temperatures of 1000°C and 1100°C the presence of spinel $(Mn,Cr)_3O_4$ and Cr_2O_3 phases can be also observed, indicating that the steel substrate oxidized under the coating at higher temperatures.

Apart from the fact that the type of oxidation products varied with experimental conditions of the oxidation tests, relative amounts of these compounds also changed. The samples of uncoated stainless steel oxidized at higher temperatures and longer times exhibit increase of the content of respective oxides with temperature and time and progressive decrease of diffraction maxima attributed to metallic iron (Figures 5a-c). Extended time of exposure in oxidative environment resulted in increasing content of $(Mn,Cr)_3O_4$ spinel and TiO_2. The content of Cr_2O_3 decreased considerably with increasing time of exposure. This is explained by gradual conversion of chromium oxide to $(Mn,Cr)_3O_4$, spinel, which at the same time decreases the total amount of Cr_2O_3, and covers the chromia by a layer of the new reaction product (spinel), thus decreasing the intensity of diffracted radiation from the Cr_2O_3 layer.

In the case of coated samples we observed that the fraction of monoclinic ZrO_2 in the coating remained

constant, irrespective of time and temperature of exposure. Moreover, at 900°C the tetragonal and monoclinic zirconia were the only phases detected by XRD, indicating protective action of the coating at this temperature. At 1000°C and 1100°C other phases also appeared, namely $(Mn, Cr)_3O_4$ spinel and TiO_2: at both temperatures the contents of these phases increased gradually with time. In comparison to uncoated steel their contents appear to be low, but one has to realize that the intensity of diffracted radiation from these phases is markedly decreased by the overlying protective coating.

In order to examine the oxidation products in more detail, the samples were also analyzed by SEM and EDS. Figures 6a-d shows oxidized surfaces of uncoated steel samples exposed to oxygen at 900°C and 1100°C. Most of the surface was covered by a non-protective oxide layer consisting of a thin base oxide and evenly distributed crystal nodules up to 10 μm in size. The microstructure and morphology of the layer changed in the course of oxidation, which was attributed to coarsening of oxide crystals at higher temperatures. After a short exposure time (24 h) the scale was rather uniform and homogeneous, consisting of well-defined crystallites. After longer exposure (96 h), coarser oxide crystals were observed. The SEM/EDS examination of the surface of oxidized steel substrates detected coarse-grained globular crystallites to be $(Mn,Cr)_3O_4$ spinel, which formed preferentially along grain boundaries of the oxide surface scale. The rest of the surface was covered by a thinner homogeneous oxide layer of Cr_2O_3.

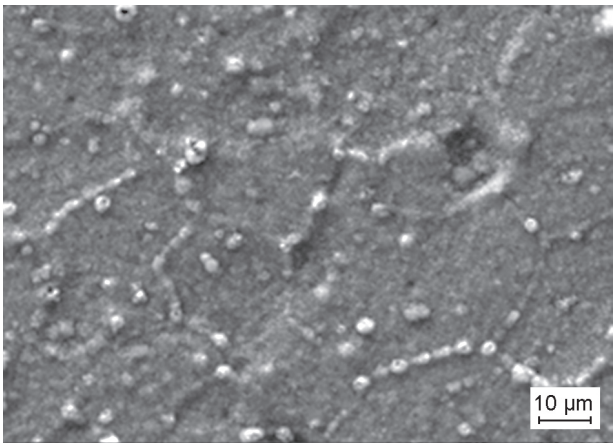

a) steel – 900°C/24 h

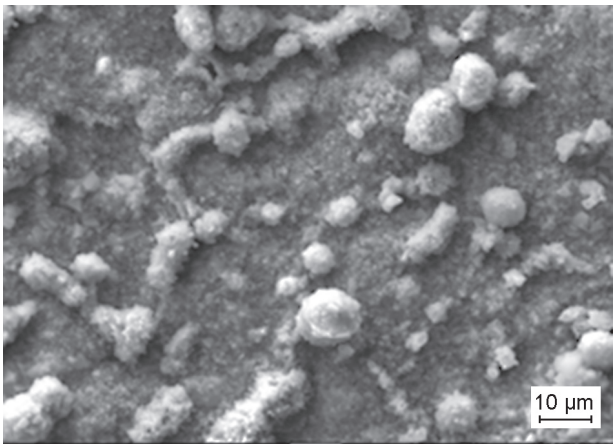

b) steel – 1000°C/24 h

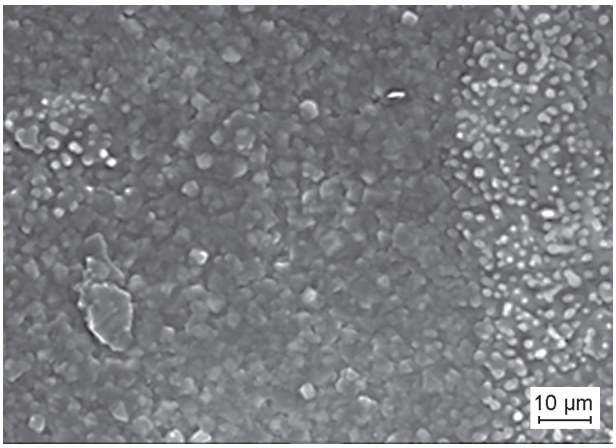

d) steel – 1100°C/24 h

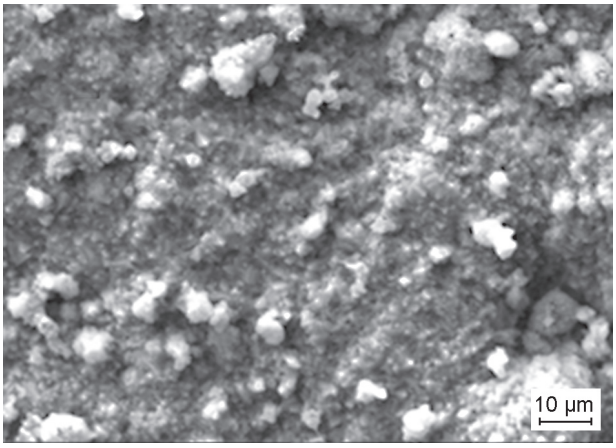

c) steel – 1000°C/96 h

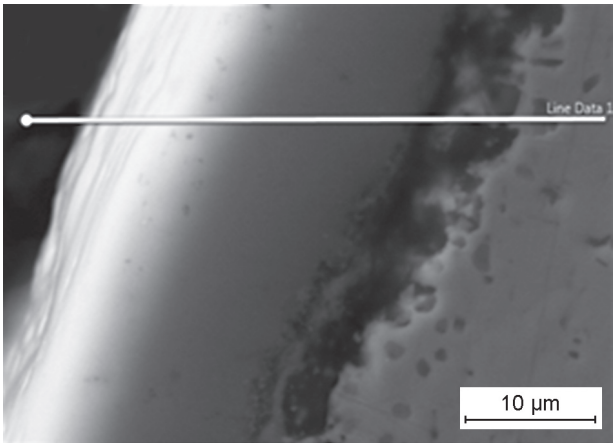

e) cross-section of steel – 1100°C/96 h

Figure 6. Microstructures of steel after corrosion tests a) steel – 900°C/24 h, b) steel – 1000°C/24 h, c) steel – 1000°C/96 h, d) steel – 1100°C/24 h, e) cross-section of steel – 1100°C/96 h.

Titanium originally present as a minor alloying element in the AISI 441 steel was also observed in oxide form, concentrated primarily in oxide precipitates between the scale and the steel substrate, but the EDS analysis indicated that some Ti was present also in the oxide scale itself. Preferential formation of the spinel phase along grain boundaries indicates that grain boundaries in the steel substrate acted as fast diffusion path for Mn and Cr. These assumptions were confirmed by examination of the cross-section morphology of corroded steel (Figure 6e, Figure 7). The EDS analysis revealed that the outer oxide layer contained relatively high amounts of chromium and manganese. The presence of a Si-enriched porous layer at the substrate/chromium oxide interface is also visible, in accord with previously published data, which reported that in the steels containing more than 0.5 % of Si, a growth of insulating, continuous or network-like films of silica can be observed under the chromia scale [36]. A zone of titanium oxide inclusions was clearly visible in the steel substrate beneath the Cr_2O_3 and silica-containing scale.

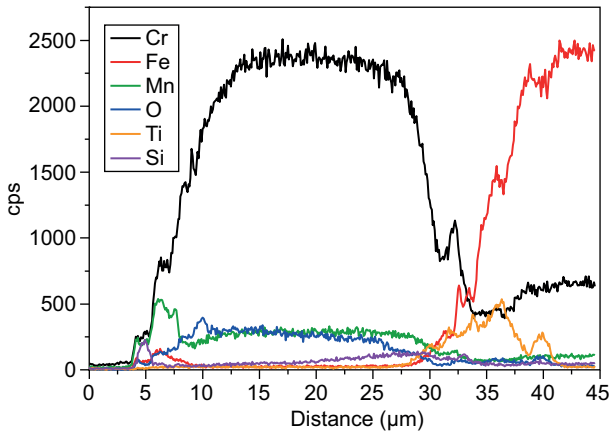

Figure 7. EDS line scan of cross-section of steel – 1100°C/96 h.

The beneficial effect of the PDC coating was observed at 900°C. While the uncoated steel was already oxidized, the coated samples were partially protected against oxidation, and the measured weight gain was only about 50 % of the weight gain of uncoated steel. The surface of the coated samples (Figures 8a-d) after oxidation tests was homogenous and, as confirmed by the XRD results, predominantly consisted of monoclinic

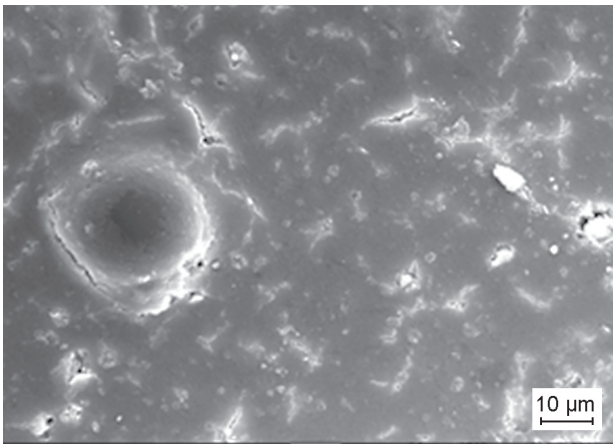

a) C 80-10-10 – 900°C/24 h

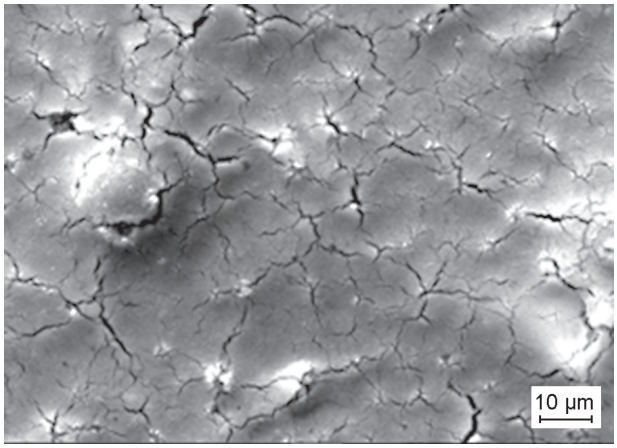

b) C 80-10-10 – 1000°C/24 h

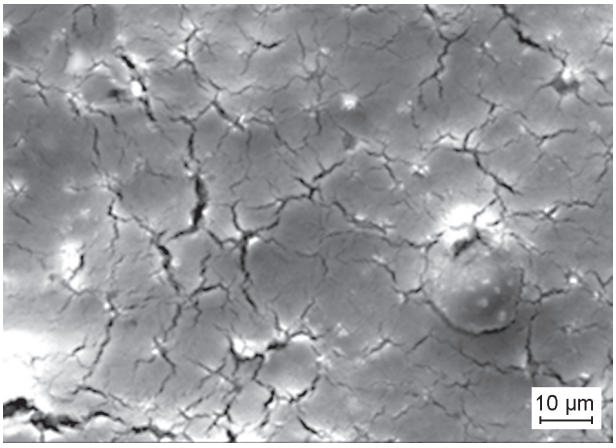

c) C 80-10-10 – 1000°C/96 h

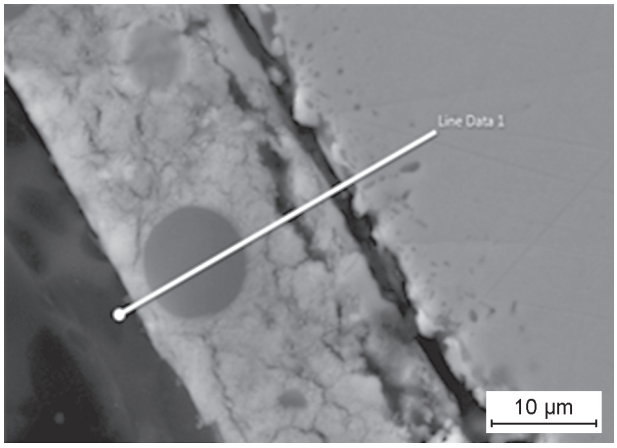

d) cross-section of C 80-10-10 – 1000°C/96 h

Figure 8. Microstructure of C-80-10-10 coating after oxidation tests: a) C 80-10-10 – 900°C/24 h, b) C 80-10-10 – 1000°C/24 h, c) C 80-10-10 – 1000°C/96 h d) cross-section of C 80-10-10 – 1000°C/96 h.

and tetragonal ZrO_2. The pull-out of glass microspheres was not observed after oxidation tests. In the samples oxidized at 1000°*C* and 1100°C the cracks present in the as-prepared coating tended to widen, most likely as the result of differential sintering of zirconia filler in the coating. The thickness of the oxide scale was reduced in comparison to uncoated steel: scale formation requires the presence of oxygen to react with metallic elements (primarily Cr, Mn) in the steel, so it is not surprising that the presence of the coating on the surface of the steel would reduce the amount of oxygen available for oxide formation, thereby reducing the scale growth rate. However, SEM cross-section analyses (Figure 8d) on PDC coated samples revealed gaps along the oxide scale/metal interface. This may be an indication of weak adherence of the scale to the steel substrate. It should also be noted that spallation of the oxide scale from the coated steel substrate was only observed on coated substrates, whereas no spallation was observed on the uncoated substrate. The EDS analysis (Figure 8d, Figure 9) also revealed the presence of Cr and Mn in the coating. As expected, the oxide scale that grew between the steel substrate and the coating were rich in Cr, with a substantial amount of Mn. This was consistent with the oxidation behaviour of uncoated ferritic stainless steels, which typically form a dual layer scale consisting of a $(Mn,Cr)_3O_4$ spinel-rich top layer and a chromia sublayer [37]. It is likely that the Cr was incorporated into the coating during the early stages of oxide film formation before a fully dense, protective chromia scale could be formed. Especially at high temperature oxidation (i.e. 1000°C and 1100°C) the porous coating serves as a gate for oxygen diffusion to steel substrate, resulting in formation of oxide layer at coating/steel interface. Unlike uncoated steel the oxide layer at the coating/metal interface spalls off, for unknown reason. Further optimization of the coating composition is required to achieve effective corrosion protection of steel substrate.

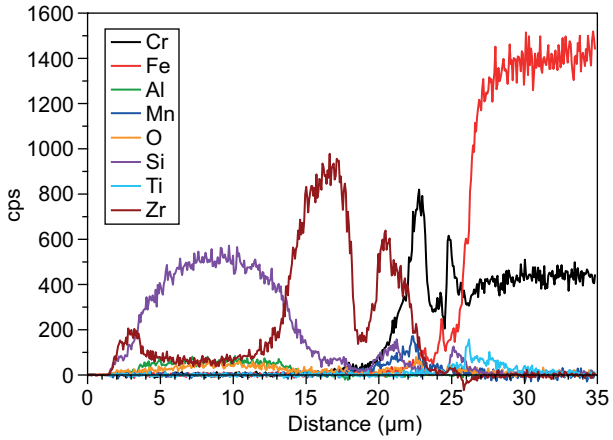

Figure 9. EDS line scan of cross-section of C-80-10-10 – – 1000°C/96 h.

CONCLUSIONS

The work was aimed at development of corrosion and oxidation resistant coating system for the AISI441 stainless steel. For that purpose, a double layer coating, consisting of a PDC bond-coat, and a PDC top-coat with ceramic and specially tailored glass fillers ($SiO_2Al_2O_3$-ZrO_2 glass) in the form of microspheres with high melting temperature were prepared and studied from the point of view of their hydrothermal corrosion and high temperature oxidation resistance. Since the prepared coatings were not fully dense, the static corrosion tests under hydrothermal conditions at 200°C did not deliver promising results. Application of the static conditions caused delamination of the bond coat from steel substrate and the failure of composite coatings. Beneficial effect of the PDC coating with the fillers in terms of oxidation protection of the steel substrate was observed at 900°C, with the mass gain about one half of that in uncoated steel oxidized under the same conditions, while at 1000°C and 1100°C no protective effect of the coating was observed. Oxidation of stainless steel substrate yielded passivation Cr_2O_3, layer with some TiO_2 and a $(Mn,Cr)_3O_4$ spinel non-protective upper layer. In coated samples monoclinic and tetragonal ZrO_2 were the dominant phases at 900°C, while at higher temperatures formation of $ZrSiO_4$ was observed within the coating, with $(Mn,Cr)_3O_4$ and Cr_2O_3 present at the coating/steel interface. Unlike uncoated steel, spallation of the Cr_2O_3 passivation layer was observed under the protective coating at higher temperatures.

Acknowledgment

Financial support of this work by the grant VEGA 2/0058/14, the grant APVV 001415, and the Alexander von Humboldt Foundation in the frame of the institutional cooperation grant scheme is gratefully acknowledged. This publication was created in the frame of the project "Centre of excellence for ceramics, glass, and silicate materials" ITMS code 262 201 20056, based on the Operational Program Research and Development funded from the European Regional Development Fund.

REFERENCES

1. Jablonski P.D, Cowen C.J., Sears J.S. (2010): Exploration of alloy 441 chemistry for solid oxide fuel cell interconnect application. *Journal of Power Sources*, *195*, 813-820. doi: 10.1016/j.jpowsour.2009.08.023
2. Badin V., Diamanti E., Forêt P., Darque-Ceretti E. (2014): Characterization of Oxide Scales Formed on Ferritic Stainless Steel 441 at 1100 °C under water vapour. *Oxidation of Metals*, *82*, 347–357. doi: 10.1007/s11085-014-9495-2
3. Badin V., Diamanti E., Forêt P., Darque-Ceretti E. (2015): Water Vapor Oxidation of Ferritic 441 and Austenitic 316L Stainless Steels at 1100°C for Short Duration.

Procedia Materials Science, *9*, 48–53. doi: 10.1016/j.mspro.2015.04.006

4. Srisrual A., Coindeau S., Galerie A., Petit J.P., Wouters Y. (2009): Identification by photoelectrochemistry of oxide phases grown during the initial stages of thermal oxidation of AISI 441 ferritic stainless steel in air or in water vapour. *Corrosion Science*, *51*, 562–568. doi: 10.1016/j.corsci.2008.12.002
5. Stott F.H., Wood G.C, Stringer J. (1995): The influence of alloying elements on the development and maintenance of protective scales. *Oxidation of Metals, 44*, 113–145. doi: 10.1007/bf01046725
6. Colombo P., Mera G., Riedel R., Sorarù G.D. (2010): Polymer-derived ceramics: 40 Years of research and innovation in advanced ceramics. *Journal of the American Ceramic Society*, *93*, 1805–1837. doi: 10.1111/j.1551-2916.2010.03876.x
7. Kappa M., Kebianyor A., Scheffler M. (2010): A two-component preceramic polymer system for structured coatings on metals. *Thin Solid Films*, *519*, 301–305. doi: 10.1016/j.tsf.2010.08.091
8. Goerke O., Feike E., Heine T., Trampert A., Schubert H. (2004): Ceramic coatings processed by spraying of siloxane precursors (polymer-spraying). *Journal of the European Ceramic Society*, *24*, 2141–2147. doi: 10.1016/S0955-2219(03)00362-5
9. Spencer K., Zhang M.X. (2011): Optimisation of stainless steel cold spray coatings using mixed particle size distributions. *Surface and Coatings Technology*, *205*, 5135–5140. doi: 10.1016/j.surfcoat.2011.05.020
10. Morlier A., Cros S., Garandet J.P., Alberola N. (2012): Thin gas-barrier silica layers from perhydropolysilazane obtained through low temperature curings: A comparative study. *Thin Solid Films*, *524*, 62–66. doi: 10.1016/j.tsf.2012.09.065
11. Cromme P., Scheffler M., Greil P. (2002): Ceramic tapes from preceramic polymers. *Advanced Engineering Materials*, *4*, 873–7. doi: 10.1179/174367609X459540
12. Günthner M., Kraus T., Dierdorf A., Decker D., Krenkel W., Motz G. (2009): Advanced coatings on the basis of Si(C)N precursors for protection of steel against oxidation. *Journal of the European Ceramic Society*, *29*, 2061–2068. doi: 10.1016/j.jeurceramsoc.2008.11.013
13. Torrey J.D., Bordia R.K. (2008): Processing of polymer-derived ceramic composite coatings on steel. *Journal of the American Ceramic Society*, *91*, 41–45. doi: 10.1111/j.1551-2916.2007.02019.x
14. Colombo P., Paulson T.E., Pantano C.G. (2005): Synthesis of Silicon Carbide Thin Films with Polycarbosilane (PCS). *Journal of the American Ceramic Society*, *40*, 2333–2340. doi: 10.1111/j.1151-2916.1997.tb03124.x
15. Kroke E., Li Y.L., Konetschny C., Lecomte E., Fasel C., Riedel R. (2000): Silazane derived ceramics and related materials. *Materials Science and Engineering*, *26*, 97–199. doi: 10.1016/S0927-796X(00)00008-5
16. Bauer F., Decker U., Dierdorf A., Ernst H., Heller R., Liebe H., Mehnert R. (2005): Preparation of moisture curable polysilazane coatings: Part I. Elucidation of low temperature curing kinetics by FT-IR spectroscopy. *Progress in Organic Coatings*, *53*, 183–190. doi: 10.1016/j.porgcoat.2005.02.006
17. Lukacs A. (2007): Polysilazane precursors to advanced ceramic. *American Ceramic Society Bulletin*, *86*, 9301-9306.
18. Günthner M., Wang K., Bordia R.K., Motz G. (2012): Conversion behaviour and resulting mechanical properties of polysilazane-based coatings. *Journal of the European Ceramic Society*, *32*, 1883–1892. doi: 10.1016/j.jeurceramsoc.2011.09.005
19. Khan N., Lu J. (2007): Thermal cyclic behavior of air plasma sprayed thermal barrier coatings sprayed on stainless steel substrates. *Surface and Coatings Technology*, *201*, 4653–4658. doi: 10.1016/j.surfcoat.2006.10.022
20. Barroso G.S., Krenkel W., Motz G. (2015): Low thermal conductivity coating system for application up to 1000°C by simple PDC processing with active and passive fillers. *Journal of the European Ceramic Society*, *35*, 3339–3348. doi: 10.1016/j.jeurceramsoc.2015.02.006
21. Greil P. (1995): Active-Filler-Controlles Pyrolysis of Preceramic Polymers. *Journal of the American Ceramic Society*, *78*, 835–848. doi: 10.1111/j.1151-2916.1995.tb08404.x
22. Günthner M., Kraus T., Krenkel W., Motz G., Dierdorf A., Decker D. (2009): Particle-Filled PHPS silazane-based coatings on steel. *International Journal of Applied Ceramic Technology*, *6*, 373–380. doi: 10.1111/j.1744-7402.2008.02346.x
23. Günthner M., Schütz A., Glatzel U., Wang K., Bordia R:K., Greißl O., Krenkel W., Motz G. (2011): High performance environmental barrier coatings, Part I: Passive filler loaded SiCN system for steel. *Journal of the European Ceramic Society*, *31*, 3003–3010. doi: 10.1016/j.jeurceramsoc.2011.05.027
24. Labrousse M., Nanot M., Boch P., Chassagneux E. (1993): Ex-polymer SiC coatings with Al_2O_3 particulates as filler materials. *Ceramic International*, *19*, 259-67. doi: 10.1016/0272-8842(93)90058-Y
25. Wang K., Günthner M., Motz G., Bordia R.K. (2011): High performance environmental barrier coatings, Part II: Active filler loaded SiOC system for superalloys. *Journal of the European Ceramic Society*, *31*, 3011–3020. doi: 10.1016/j.jeurceramsoc.2011.05.047
26. Wang K., Unger J., Torrey J.D., Flinn B.D., Bordia R.K. (2014): Corrosion resistant polymer derived ceramic composite environmental barrier coatings. *Journal of the European Ceramic Society*, *34*, 3597–3606. doi: 10.1016/j.jeurceramsoc.2014.05.036
27. Torrey J.D., Bordia R.K. (2008): Mechanical properties of polymer-derived ceramic composite coatings on steel. *Journal of the European Ceramic Society*, *28*, 253–257. doi: 10.1016/j.jeurceramsoc.2007.05.013
28. Kraus T., Günthner M., Krenkel W., Motz G. (2009): cBN particle filled SiCN precursor coatings. *Advances in Applied Ceramics*, *108*, 476–482. doi: 10.1179/174367609X422153
29. Garvie R.C., Nicholson P.S. (1972): Phase analysis in zirconia systems. *Journal of the American Ceramics Society, 55*, 303–5. doi: 10.1111/j.1151-2916.1972.tb11290.x
30. Toraya H., Yoshimura M., Somiya S. (1984): Calibration curve for quantitative analysis of the monoclinic–tetragonal ZrO_2 system by X-ray diffraction. *Jounal of the American Ceramics Society*, *67(6)*, 119–21. doi: 10.1111/j.1151-2916.1984.tb19715.x
31. Wagner C. (1952): Theoretical Analysis of the Diffusion Processes Determining the Oxidation Rate of Alloys. *Jounal of the Electrochemical Society*, *99*, 369-380. doi: 10.1149/1.2779605
32. Geßwein H., Pfrengle A., Binder J.R., Haußelt J. (2008): Kinetic model of the oxidation of $ZrSi_2$ powders. *Journal*

of Thermal Analysis and Calorimetry, *91*, 517–23. doi: 10.1007/s10973-007-8461-5

33. Cox M.G.C., Mccenaney V.D. (1972): A chemical diffusion model for partitioning of transition elements in oxide scales on alloys. *Philosophical Magazine*, *26*, 839. doi: 10.1080/14786437208226960
34. Wild R.K. (1977): High temperature Oxidation of Austenitic Stainless Steel in Low Pressure Oxygen. *Corrosion Science*, *17*, 87-104. doi: 10.1016/0010-938X(77)90011-7
35. Lobnig R.E., Schmidt H.P., Hennesen K., Grabke H.J. (1992): Diffusion of cations in chromia layers grown on iron-base alloys. *Oxidation of metals*, *37*, 81-93. doi: 10.1007/bf00665632
36. N'Dah E., Tsipas S., Hierro M.P., Pérez F.J. (2007): Study of the cyclic oxidation resistance of Al coated ferritic steels with 9 and 12%Cr. *Corrosion Science*, *49*, 3850. doi: 10.1016/j.corsci.2007.05.011
37. Yang Z., Xia G.G., Wang CH.M., Nie Z., Templeton J., Stevenson J.W., Singh P. (2008): Investigation of iron–chromium–niobium–titanium ferritic stainless steel for solid oxide fuel cell interconnect applications. *Journal of Power Sources*, *183*, 660-667. doi: 10.1016/j.jpowsour.2008.05.037